CrossMark

RESEARCH ARTICLE - CHEMISTRY

Synthesis of Transparent Amorphous Carbon Thin Films from Cellulose Powder in Rice Straw

Mahmoud Fathy[1] · Th. Abdel Moghny[1] · Mahmoud Ahmed Mousa[2] ·
Abdel-Hameed A-A. El-Bellihi[2] · Ahmed E. Awadallah[3]

Abstract The transparent amorphous carbon thin films (ACTF) were prepared through a batch acid spraying technique in the presence of cobalt silicate as a catalyst at low temperature between 30 and 45 °C. Hence, the catalyst was prepared using silica gel as a basic matrix and supporting material to produce ACTF. The produced active carbon was characterized using XRD, FTIR, and Raman spectrum. The high-resolution transmission electron microscope (HR-TEM) and thermogravimetric analysis were used to analyze the surface morphology and thermal stability of cellulose and ACTF, whereas the surface area was calculated using the standard iodine method. The results of Raman spectroscopy and TEM show the realization of ACTF suspension with highest constitutional order and the lowest number of layers with confirming of the succeed preparation of thin ACTF layers in thickness and average size of 1 and 100 mm, respectively. In addition, under these conditions, the activated carbons' iodine value is 721.64 mg/g, and the yield ratio is 85.71 %.

Keywords Carbon materials · Amorphous materials · Functional · Porous materials · Thin films

✉ Mahmoud Fathy
  fathy8753@yahoo.com

1   Applications Department, Egyptian Petroleum Research
    Institute (EPRI), 1 Ahmed El-Zomer, Nasr City, Box. No.
    11727, Cairo, Egypt

2   Faculty of Science Benha University, Fred Nada Street,
    Banha, Cairo, Egypt

3   Development of Processes Department, Egyptian Petroleum
    Research Institute, 1 Ahmed El-Zomer, Nasr City, Box. No.
    11727, Cairo, Egypt

1 Introduction

Pitch and coke are the two individual relevant materials for getting different carbons resources, such as carbon blacks, carbon filaments, and activated carbons (ACs). Such carbon resources are not economical, and given their restricted stores besides the rise of their production cost, an alternative starting materials, such as coffee lees, tri-acetyl cellulose waste, and oak woods, to produce carbon nanomaterials like AC were proposed by [1].

Rice straw as abundant agricultural residues was involved in different industries and molding process such as the production of nanosilica having high specific surface area, high gas absorbability, and high oil absorption. The cellulose material in rice straw represents 55 % of the total material mass and found in amorphous or crystalline forms [2,3]. Therefore, in the future, many of the world's scientific studies can be exploited by creating new technologies based on cellulose, [4–7].

The unique properties of carbon nanomaterials such as the large surface areas and the unusual electronic structure are one of the subsidiary factors qualified it as adsorbed materials and to be utilize in halocarbon disintegration, extraordinarily chlorocarbon, and pesticide evacuation; also, carbon nanomaterials have been adaptable carbon to utilize for water filtration and desalination [8–10]. Amorphous carbon is permeable carbon materials for many applications such as toxins absorbent in vaporous phase or fluid stage like adsorbent electrode for electrosorption-based uranium extraction from seawater; hence, the extracted uranium supports the use of nuclear power as a sustainable generating technology [11,12]. Another use for amorphous carbons is a modification of commercial activated carbon for the removal of 2, 4-dichlorophenol from synthetic wastewater [13] and gas' capacity and as impetuses backing.

Springer

Carbon nanomaterials like ACTF need to enhance to be similar to graphite upheavals. To realize many potential applications of graphene, we need a scalable method for transferring graphene from the metal film or foil growth substrate such as Cu or Ni to application-specific substrates.

Graphene is most commonly transferred from the metal growth substrate by deposited it on polymer film, such as polymethyl methacrylate (PMMA) or polydimethylsiloxane (PDMS) on the top of graphene [14,15]. This allows etching of the metal to free the polymer-supported graphene for transfer to the desired surface, followed by mechanical transfer to the target surface. Graphene removal from metal has alternatively been achieved by depositing epoxy on the graphene followed by mechanical peeling [16,17]. This approach also requires dissolution of the sport and can result in an incomplete transfer.

Today carbon nanostructure got from plant cellulose is the most general and appropriate adsorption medium utilized for water refinement. Propelled methods [18,19], for example film filtration, reverse osmosis, and particle trade, can be used as a part of treatment and water desalination [20–22]. The joining of carbon nanostructure on inorganic surfaces and a resulting concoction treatment could change it to graphene carbon (GC). Hence, the activation of carbon nanostructure may produce highly effective adsorbents [23,24].

This paper focus on synthesized of transparent amorphous carbon thin film containing amorphous honeycomb-shaped networks, self-assembled on the cobalt silicate template using in situ chemical treatment based on cellulosic material. We report the direct fabrication of ACTF on $CoSiO_2$ nanoparticles by growth of interfacial ACTF between Co and SiO_2, followed by dry mechanical removal of the Co silicate nanoparticles from the substrate.

2 Experimental

2.1 Materials

Rice's straw powdered was obtained from Egypt and characterized by 60–80 meshes and stored in reagent glass. Sulfuric acid, cobalt acetate, and silica powders were from Sigma-Aldrich.

2.2 Instrumentation

XRD characterization was performed using X-ray diffractometer system (D/MAX 2200H, Bede 200, Rigagu Instruments C).

The FTIR spectrum (1000–2000 cm^{-1}) was measured using Thermo scientific FTIR spectrometer with pure KBr as the background. The samples were mixed with KBr, and the mixture was dried and compressed into a transparent tablet

for measurement. The surface morphology of all the samples was analyzed using high-resolution transmission electron microscope (HR-TEM, FEI Titan 80-300).

Raman spectra were obtained using Renishaw 1000/2000 spectrometers with a HeNe laser ($\lambda = 633$ nm) for the ACNN with a laser spot around 1–2 μm in diameter, using the so-called VV polarization configuration, where the polarization of incident and scattered radiation is parallel to each other.

2.3 Methods

2.3.1 Preparation of Cobalt Silicate Nanoparticles

A cobalt silicate nanoparticle was prepared by vigorously stirring of 4.0 g cobalt acetate and silica with 200 ml of ethanol for 30 min at 45 °C, after that 40 ml water and 4 ml (1.4 M) NaOH were added to the above suspension. Then, the powder was separated and being too dry at 50 °C for 8 h in a vacuum oven.

2.3.2 Rice Straw Pretreatments

Rice straw was subjected to the pretreatment process. Hence, hemicellulose was solubilized in the form of monomeric sugars during the dilute acidic hydrolysis process using 1 % (wt/wt) sulfuric acid at 120 °C for 60 min [25,26]. Following that succeeding, delignification process was carried out at 120 °C for 60 min using a mixture of 1.5 % (wt/wt) NaOH and 0.5 % (wt/wt) H_2O_2 to remove lignin and silica present in rice straw, after that the black liquor residue was obtained.

2.3.3 Chemical Exfoliation of Cellulose

A catalytic acid spraying method (CAS) was started by mixing and stirring for 10 min of 5 g cellulose with 5 ml concentrated sulfuric acid in the presence of 0.1 g silica. Then, 4–5 batches were sprayed at a rate of 2 ml/minute with an interval of 5 min between each batch. Then filtrated and washing with hot water until pH 7 and saving in the oven at 40 °C for 6 h. The prepared amorphous carbon thin film (ACTF) was poured in a flask in the presence of 0.01 g cobalt silicate nanoparticles and heated up to 40 °C for 30 min. The prepared carbon nanomaterials left to cool for 1 h and then dried in a vacuum oven for 24 h at 50–70 °C [27].

2.3.4 Iodine Number (IN) Test

10 mL of 5 % (V/V) HCl was used to treat the ACTF sample. The mixture boiled for 30 s and cooled to room temperature. Then, 100 mL of 0.1N iodine solution is immediately added to the mixture and stirred for 30 s. The solution is then filtered, and 50 mL of the filtrate is titrated with 0.1N (0.05 mol
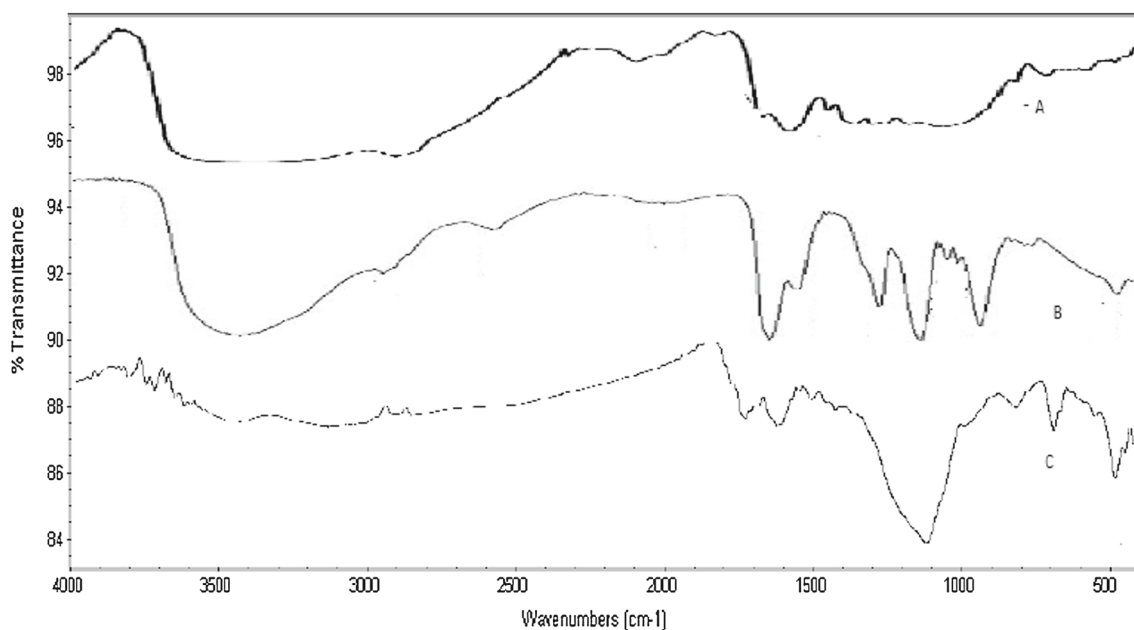
Fig. 1 FTIR of **a** rice straw, **b** microcrystalline cellulose, and **c** ACTF

L^{-1}) sodium thiosulphate solution using starch as an indicator. The amount of iodine adsorbed per gram of adsorbent is plotted against the residual iodine concentration, using logarithmic axes. If the residual iodine concentration is not within the range of (0.008–0.04 N), the procedure is repeated using different carbon masses for each isotherm point. A regression analysis is applied to the three points, and the iodine number is calculated as the amount adsorbed at a residual iodine concentration of 0.02 N.

3 Results

3.1 FTIR Analysis

FTIR spectroscopic analysis of initial rice straw samples in Fig. 1a shows the presence a broadband at 3600–3100 cm^{-1} which indicates the presence of OH-stretching vibration concerning to presence of hydrogen bonds and band at 2900 cm^{-1} corresponding to the C–H stretching vibration. The low-intensity adsorption bands at 1500–899 cm^{-1} region represents the presence of C–O bond [28,29], whereas the FTIR spectroscopic of microcrystalline cellulose in Fig. 1b shows the same broadband at 3600–3100 cm^{-1} which indicates the presence of OH^{-} stretching vibration, but became sharper and lower intensity as compared to the initial cellulose samples (Fig. 1b), which can be correlated with the scission of the intra- and intermolecular hydrogen bonds [30]. In addition, a strong conjugated C=C peak was observed around 1633.83–1638.32 cm^{-1}. This sample as well shows four prominent absorption peaks at 1251.06, 1160.53, 1113.89,

and 1053.53 cm^{-1},respectively, which represent the stretching of C–O functional group.

FTIR spectra of ACTF in Fig. 1c show a strong and broad absorption peak appeared at 3434.06 cm^{-1}, which corresponds to the stretching of O–H functional group, and this shows the presence of bonded hydroxide in the untreated sample. There was another peak observed at 2930.44 cm^{-1} corresponding to the C–H sp3 stretching. All the examples show a broad rocky peak around 3425.12–3440.32 cm^{-1}, which indicates the presence of OH in the samples. It is most probably of the R-OH bonded like molecule in carbon.

3.2 Raman Analysis

Raman spectra of transparent amorphous carbon thin films (TACTF) are given in Fig. 2, the spectrum displayed broadened prominent G peak at 1592 cm^{-1}, and that peak was shifted corresponding to the first-order scattering of E_{2g} mode from 1582 cm^{-1}. Also, the D band at 1363 cm^{-1} becomes sheltered which indicates the reduced size of the in-plane sp^2 domains, possibly due to the extensive oxidation [31–33]. The intensity ratio ID/IG continuously decreases after the thermal treatment at 285 K, indicating the rearrangements of the carbon atoms to reduce structural defects and thus to improve the graphitization of the ACTF. This change suggests a decrease in the average size of the sp^3 upon oxidation of the exfoliated graphite nanoparticles, and the value of $I_{\mathrm{D}}/I_{\mathrm{G}} = 0.333$ is the ratio of amorphous or defect peak to the graphenic one which indicates the highly succeed preparation of TACTF with a high degree of crystallinity and low defecates.
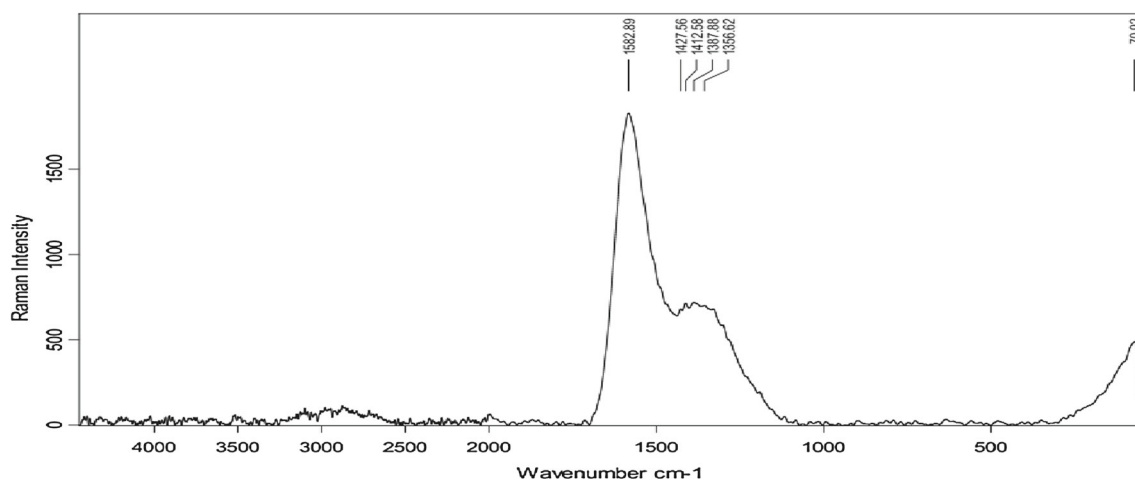
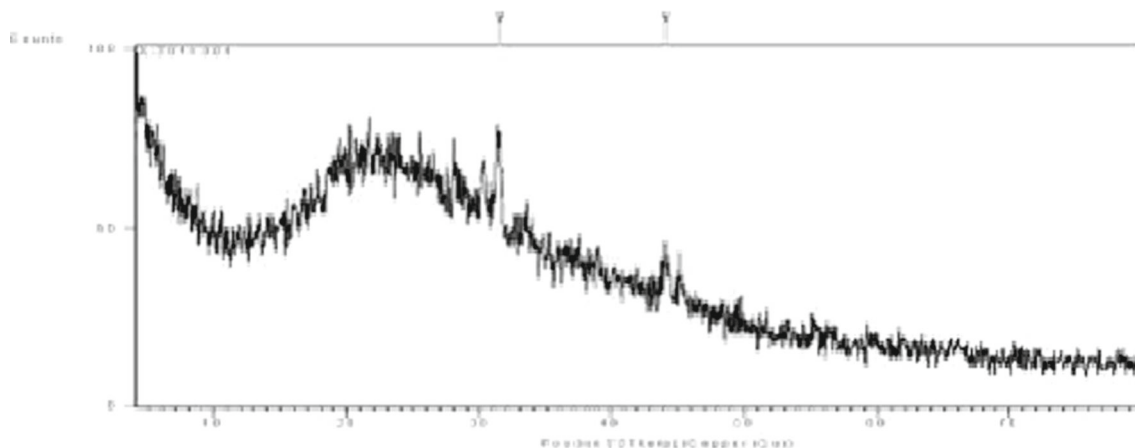**Fig. 2** Raman analysis of thin film amorphous carbon

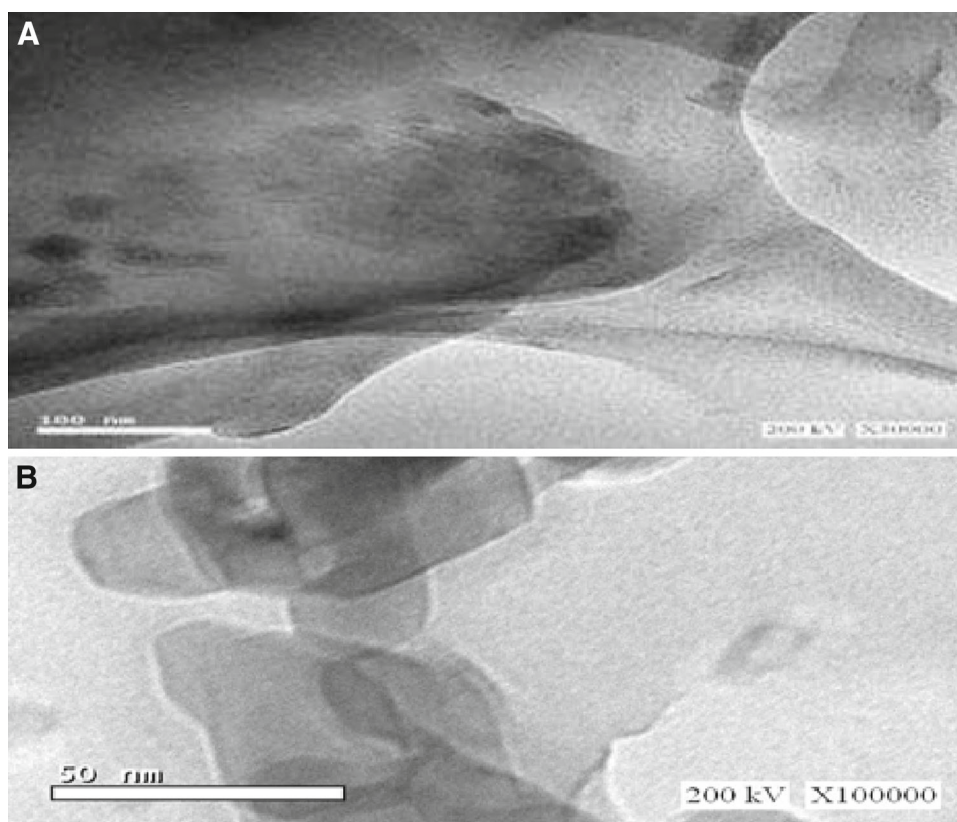**Fig. 3** XRD transparent amorphous carbon thin films

The contribution of D and G bands from the fittings showed peak sharpening with the oxidative treatment and the heat treatment as observed from the full width at half maximum (FWHM). The oxidative process and heat treatment at the 285 K show that the FWHM of the D band showed a more drastic decrease compared to the G and D bands.

3.3 X-ray Diffraction Analysis

In Fig. 3, the X-ray pattern shows that the amorphous carbon thin films record peaks of 20°, 25°, and 40°, at 2θ, and this indicated the presence of high clear crystalline amorphous carbon thin films corresponding to graphite structure of transparent amorphous carbon thin films. Such XRD spectra also illustrate the successful preparation of carbonized ACTF from a cellulosic material. In the XRD patterns of ACTF, the broadness of the diffraction peaks indicates the

presence of disorder in their periodic structures. To investigate the effect of using the chemical treatment as a template process for the carbon materials, we compared the structural properties of ACTF sample with the increase in cellulose contents; these carbon materials carbonized from the chemical treatment have increased intensity peaks of ACTF with the highest intensity of the peaks at 20°. The amorphous peak at 20° indicated the presence of silica nanoparticles at sizes reached to 50 nm, which indicate the presence of transparent amorphous carbon thin films peaks [34]. It is known that the decreases in the size of the prepared nanoparticles lead to appear of the broad amorphous band more than original crystalline one. Meanwhile, the XRD spectra of the prepared ACTF from cellulose at 65 % H_2SO_4 seem a high crystalline. This might indicate that the prepared ACTF is similar in its grade and standard to that the commercial carbon.

Fig. 4 HRTEM of **a** transparent amorphous carbon thin films and **b** cobalt silicate catalysis

3.4 The High-Resolution Transmission Electron Microscope (HR-TEM) and Selected Area Electron Diffraction (SAED) analysis

HR-TEM images Fig. 4-a revealed that the transparent amorphous carbon thin films consist of irregular aggregated, thin, crumpled sheets closely associated with each other and forming a disordered solid. The folded regions of the sheets have average widths of 2 nm which indicate the presence of individual layers in the prepared transparent amorphous carbon thin films. Furthermore, suggest that the preparation of transparent amorphous carbon thin films using a new chemical treatment process in the presence of cobalt silicate nanoparticle giving highly ordered amorphous graphene sheets with the small crosslinked layer above and lower the original graphene sheet.

The morphology, size, and dispersion of cobalt silicate nanoparticles prepared in O/W and W/O micro emulsion were characterized by HR-TEM as shown in Fig. 4b. The micrograph shows that the prepared Co NPs are very small and cubic or spherical form, and their particle size distribution was uniform ($\sim$30 nm). Also, the HR-TEM images in Fig. 4b detected NPs agglomeration of four selected cobalt catalysts prepared by doping of cobalt in silica by showing different particle size distributions. It found that the optimum amount of doping 20 wt% CoO_2 leads to produce of Co nanoparticles with major size between 30 and 50 nm.

The SAED pattern in Fig. 5 shows only weak and thin rings, indicating that the prepared transparent amorphous carbon thin films are in the amorphous structure form. It is expected that the stacking sheets of transparent amorphous carbon thin films are due to van der Waals's attractive interactions, with a random arrangement.

3.5 Thermal Analysis

Figure 6 demonstrates that the thermal properties of cellulose and amorphous carbon thin film appeared as raw material. As can be seen, the initial mass losses starting at $\sim$25 °C for cellulose, and the amorphous carbon thin film (due to high solvation capacity with water molecule) showing evaporation of loose surface bound moisture (H_2O) [35]. The intramolecularly H-bonded of water is evaporated at near about 120 °C for all two samples. The degradation of cellulose starts forward at 270 °C, and the rate of degradation reaches its maximum peak at 400 °C while that of amorphous carbon thin film occurs at 288 °C and the rate of degradation becomes maximum at 600 °C.

3.6 SEM Analysis

The SEM morphological image of amorphous carbon thin film synthesized from rice straw in Fig. 7 shows the riche and

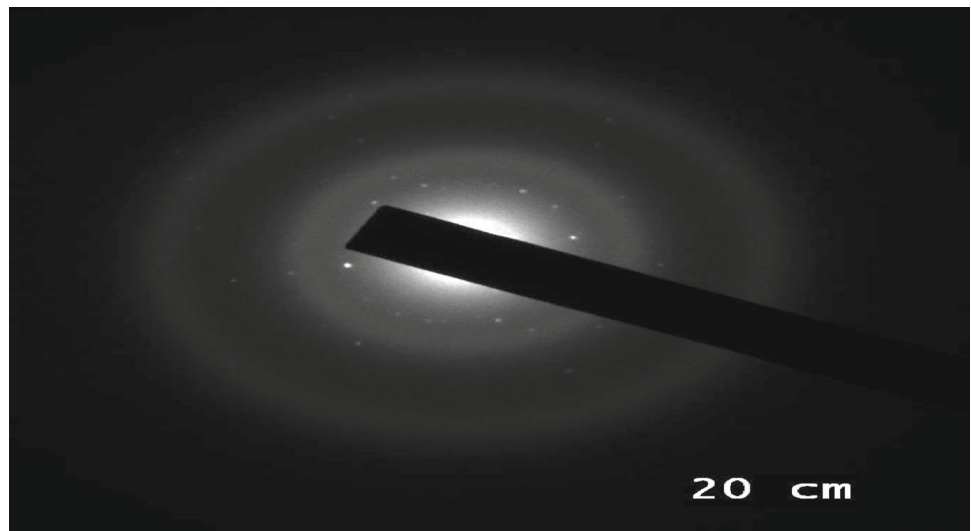**Fig. 5** SAED of transparent amorphous carbon thin films

Fig. 6 TGA analysis of cellulose and the amorphous carbon thin film
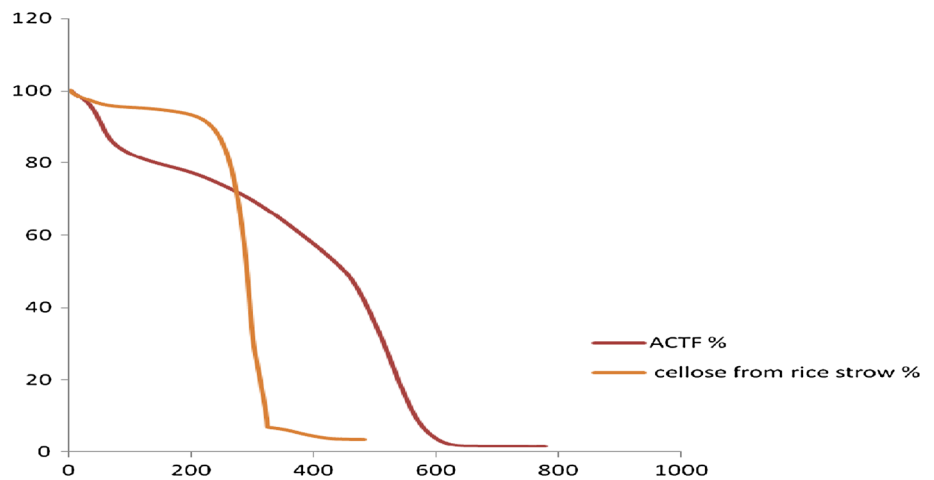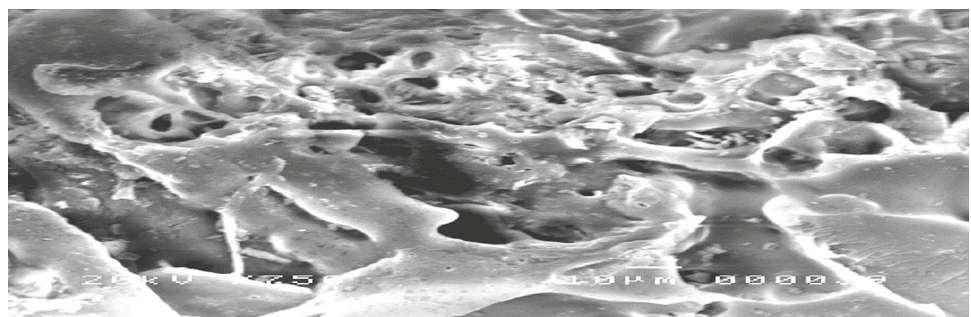

Fig. 7 SEM of amorphous carbon thin film from rice straw

best porous structure in external surface due to the presence of cobalt silicate and acid reagent. On the other hand, when comparing the SEM morphological surface of the physically activated carbon we did not find any porous structure except for any occasional cracks as reported in some literature. This my due to that the acidic groups found on the surface of ACTF could give numerous adsorption sites and therefore increase ACTF adsorption capacities for Na^+ ions. In addition, the morphology image illustrated that the ACTF adhere to each other; therefore, the interspaces between ACTF are significantly reduced. Based on our recent SEM analysis, the presence of interparticle repulsion forces due to carboxylic groups on the surface of ACTF in smaller-sized "globs"of ACTF resulting a smaller ACTF aggregates of carboxyl-

Table 1 Different values of Surface areas of AC according to iodine number test

Sample	Surface area (mg/g)
Pot. Hydroxide	493.85
Phosphoric acid	423.3
Thermal activation	522.07
Eucarbon	592.62
Acid treatment (Co silicate)	1000

functionalized ACTF. This feature shows that it is possible to use the functioned ACTF as adsorbents in the treatment of polluted water and sewer water.

3.7 Adsorption Capacity of ACTF

The measurement of the iodine number can be utilized to identify roughly the surface area of activated carbon at room temperature. It is shown that the SIN method can be used for a quick estimation of the structural development of porous carbonaceous materials. An iodine number of 900 for an activated carbon is a decent grade. A more sumptuous grade of the new activated carbon thin film has an iodine number of more preponderant than 1000 mg/g, and that very valid result that observed in that modern carbon material. As shown in Table 1, the best surface area of the ACTF after the iodine number test was gotten utilizing acid treatment with cobalt silicate catalysis as an activating agent, which delivered 1000 mg/g as surface area [36].

3.8 Rule of Cobalt Silicate in the Production of the ACTF

There are different ways to create or isolate of graphene monolayers, but for ACTF, there are a few ways or not. Chemical treatment is a method that can produce potentially and relatively high quality of ACTF on a large scale. The chemical treatment process is reasonably straightforward, although some specialist equipment is necessary to create a good quality of ACTF [37].

Chemical treatment in acid media to synthesize of CTF using Co silicate as a transition metal substrate is a new method. In fact, it was a relatively new technique compared to mechanical exfoliation and the desorption of Si from single-crystal SiC [38,39]. There are a lot of research activities using Co to grow single-layer graphene and transfer graphene onto an insulating substrate for device fabrication and testing, but for the production of amorphous ACTF from cellulosic materials is under study.

ACTF on Co is grown by the decomposition of cellulose in the dilute acid over the surface at 35–40 °C. The thickness of the Co substrate is usually 25–50 nm. For a typical growth process, the Co foil has first annealed at 40 °C in an ethanol environment with silica for 30 min. Then, a few cellulose materials as the carbon source are introduced for about 30 min. Figure 8 illustrates the proposed growth mechanism of ACTF on Co silicate. The annealing at low temperature is to remove the native oxide layer on the Co surface while Co silicate grains will also develop. With the exposure of Co foil in cellulose materials environment, nucleation of ACTF islands starts taking place randomly, but preferentially at the
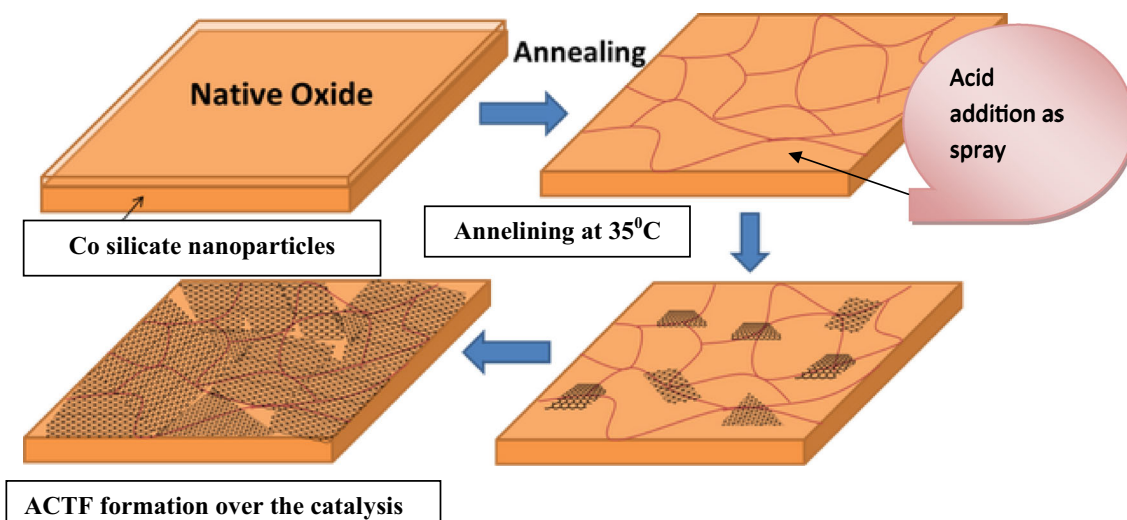

Fig. 8 Schematic illustrating the proposed growth mechanism of ACTF on Co substrates by chemical treatment: **a** couplet silicate nanoparticles with native oxide; **b** native Co oxide is a grains on the surface after annealing at 35 °C temperature; **c** the exposure of the Co foil to cellulose at 40 °C leading to the nucleation of ACTF islands; **d** enlargement of the ACTF flakes and coalescence of ACTF domains with different lattice orientation

grain boundary of Co silicate surface. As the exposure to cellulose materials continues, the ACTF domains grow to cover the whole area of Co silicate substrates and eventually aggregate into a continuous ACTF.

4 Conclusion

This study identified sulfuric acid in the presence of cobalt silicate nanoparticles as the reagent among other mineral acids for the production of carbon nanoparticles from the cellulose material. The chemical and crystalline structures of cellulose and transparent amorphous carbon thin films have been proved using FTIR and XRD analysis. The prepared transparent amorphous carbon thin film was clarified using HR-TEM and SAED and indicated that the thickness of the transparent amorphous carbon thin films has very high-purity thin sheet with amorphous crosslinked cilia; therefore, the ratio of carbon material to the original cellulose sample reaches to 60 %.

References

1. Kawahara, Y.; et al.: Activated carbon production by co-carbonization of feathers using water-soluble phenolic resin under controlled graphitization. Sustain. Mater. Technol. **4**, 18–23 (2015)
2. Gomaa, R.; et al.: Usage of treated rice straw with exogenous anaerobic bacterial enzymes (ZAD) for Ossimi sheep. Ann. Agric. Sci. **57**(2), 183–190 (2012)
3. Zuluaga, R.; et al.: Cellulose microfibrils from banana rachis: effect of alkaline treatments on structural and morphological features. Carbohydr. Polym. **76**(1), 51–59 (2009)
4. Chen, W.-H.; et al.: Ethanol production from rice straw hydrolysates by Pichia stipitis. Energy Procedia **14**, 1261–1266 (2012)
5. Xiong, S.; Wang, Q.; Xia, H.: Preparation of polyaniline nanotubes array based on anodic aluminum oxide template. Mater. Res. Bull. **39**(10), 1569–1580 (2004)
6. Jabasingh, S.A.; et al.: Catalytic conversion of sugarcane bagasse to cellulosic ethanol: TiO2 coupled nano-cellulose as an efficient hydrolysis enhancer. Carbohydr. Polym. **136**, 700–709 (2016)
7. El Nemr, A.; et al.: Synthesis of cellulose triacetate from cotton cellulose by using NIS as a catalyst under mild reaction conditions. Carbohydr. Polym. **130**, 41–48 (2015)
8. Turchanin, A.; Gölzhäuser, A.: Carbon Nanomembranes from self-assembled monolayers: functional surfaces without bulk. Prog. Surf. Sci. **87**(5–8), 108–162 (2012)
9. Karimi, A.; et al.: Functional group effect on carbon nanotube (CNT)-supported cobalt catalysts in Fischer–Tropsch synthesis activity, selectivity, and stability. Fuel **117, Part B**(0), 1045–1051 (2014)
10. Zsófi, Z.; et al.: Texture characteristics of the grape berry skin and seed (Vitis vinifera L. cv. Kékfrankos) under post veraison water deficit. Sci. Hortic. **172**, 176–182 (2014)
11. Zong, E.; et al.: Adsorptive removal of phosphate ions from aqueous solution using zirconia-functionalized graphite oxide. Chem. Eng. J. **221**, 193–203 (2013)
12. Ismail, A.F.; Yim, M.-S.: Investigation of activated carbon adsorbent electrode for electrosorption-based uranium extraction from seawater. Nucl. Eng. Technol. **47**(5), 579–587 (2015)
13. Anisuzzaman, S.M.; et al.: Modification of commercial activated carbon for the removal of 2,4-dichlorophenol from simulated wastewater. J. King Saud Univ. Sci. **27**(4), 318–330 (2015)
14. D'Angelo, D.; et al.: Electron-energy-loss spectra of graphene oxide for the determination of oxygen functionalities. Carbon **93**, 1034–1041 (2015)
15. Li, C.; et al.: Transformation of hydroquinone to benzoquinone mediated by reduced graphene oxide in aqueous solution. Carbon **89**, 74–81 (2015)
16. Lock, E.H.; et al.: Dry graphene transfer print to polystyrene and ultra-high molecular weight polyethylene: detailed chemical, structural, morphological and electrical characterization. Carbon **86**, 288–300 (2015)
17. Wu, J.; et al.: Multilayered silicon embedded porous carbon/graphene hybrid film as a high-performance anode. Carbon **84**, 434–443 (2015)
18. Struzzi, C.; et al.: High-quality graphene on single crystal Ir(1 1 1) films on Si(1 1 1) wafers synthesis and multi-spectroscopic characterization. Carbon **81**, 167–173 (2015)
19. Zhao, S.; Xue, J.: Modification of graphene supported on SiO2 substrate with swift heavy ions from atomistic simulation point. Carbon **93**, 169–179 (2015)
20. Zhu, C.; et al.: Enhanced removal of Cu(II) and Ni(II) from saline solution by novel dual-primary-amine chelating resin based on anion-synergism. J. Hazard. Mater. **287**, 234–242 (2015)
21. Zhu, J.; et al.: Preparation and characterization of negatively charged PES nanofiltration membrane by blending with halloysite nanotubes grafted with poly (sodium 4-styrenesulfonate) via surface-initiated ATRP. J. Membr. Sci. **465**, 91–99 (2014)
22. Zhu, A.; Christofides, P.D.; Cohen, Y.: On RO membrane and energy costs and associated incentives for future enhancements of membrane permeability. J. Membr. Sci. **344**(1–2), 1–5 (2009)
23. Matsumoto, S.; Shinjoh, H.: Dynamic behavior and characterization of automobile catalysts. In: Guy, B.M. (ed.) Advances in Chemical Engineering, pp. 1–279. Academic Press, London (2007)
24. Cheng, W.; et al.: Study on the corrosion properties of nanocrystalline nickel electrodeposited by reverse pulse current. Appl. Surf. Sci. **276**, 604–608 (2013)
25. Zhu, S.; et al.: Pretreatment by microwave/alkali of rice straw and its enzymic hydrolysis. Process Biochem. **40**(9), 3082–3086 (2005)
26. Zhao, R.; et al.: Methane production from rice straw pretreated with a mixture of acetic–propionic acid. Bioresour. Technol. **101**(3), 990–994 (2010)
27. El-Sayed, M.; Ramzi, M.; Hosny, R.; Fathy, M.; Moghny, T.A.: Breakthrough curves of oil adsorption on novel amorphous carbon thin film. Water Sci. Technol. **73**(10), 2361–2369 (2016)
28. Zhanjiang, P.; et al.: High-solid anaerobic co-digestion of food waste and rice straw for biogas production. J. Northeast Agric. Univ. (English Edition) **21**(4), 61–66 (2014)
29. Zhang, Q.; Cai, W.: Enzymatic hydrolysis of alkali-pretreated rice straw by Trichoderma reesei ZM4-F3. Biomass Bioenergy **32**(12), 1130–1135 (2008)
30. Yang, L.; et al.: Effects of sodium carbonate pretreatment on the chemical compositions and enzymatic saccharification of rice straw. Bioresour. Technol. **124**, 283–291 (2012)
31. Vadakkekara, R.; Chakraborty, M.; Parikh, P.A.: Room temperature benzaldehyde oxidation using air over gold–silver nanoalloy catalysts. J. Taiwan Inst. Chem. Eng. **50**, 84–92 (2015)
32. Zubir, N.A.; et al.: Optimisation of graphene oxide–iron oxide nanocomposite in heterogeneous Fenton-like oxidation of Acid Orange 7. J. Environ. Chem. Eng. **2**(3), 1881–1888 (2014)

33. Zinadini, S.; et al.: Preparation of a novel antifouling mixed matrix PES membrane by embedding graphene oxide nanoplates. J. Membr. Sci. **453**, 292–301 (2014)

34. Wu, Q.-Q.; et al.: Optimization and kinetic analysis on the sulfuric acid: catalyzed depolymerization of wheat straw. Carbohydr. Polym. **129**, 79–86 (2015)

35. Yeon, S.-H.; et al.: Enhanced anode performance of micro/mesoporous reduced graphene oxide prepared from carbide-derived carbon for energy storage devices. Carbon **91**, 241–251 (2015)

36. Jodeh, S.; et al.: Adsorption of diclofenac from aqueous solution using *Cyclamen persicum* tubers based activated carbon (CTAC). J. Assoc. Arab Univ. Basic. Appl. Sci. **20**, 32–38 (2016)

37. Omri, A.; Benzina, M.: Removal of manganese(II) ions from aqueous solutions by adsorption on activated carbon derived a new precursor: ziziphus spina-christi seeds. Alex. Eng. J. **51**(4), 343–350 (2012)

38. Zych, Ł.; et al.: The manufacturing and properties of a nanolaminate derived from graphene powder. Carbon **95**, 809–817 (2015)

39. Zhang, F.; et al.: Pyrolytic carbon-coated Si nanoparticles on elastic graphene framework as anode materials for high-performance lithium-ion batteries. Carbon **82**, 161–167 (2015)